High-Frequency Observation of Natural Disasters by SAR Interferometry

Marco D'Errico, Antonio Moccia, and Sergio Vetrella

Abstract

Synthetic Aperture Radar (SAR) interferometry is considered one of the most promising techniques for global topographic mapping. The additional potential of electronically steering the antenna range beam allows a significant increase in the observation frequency of selected areas, which is required for natural disaster monitoring and management and for observing time-varying phenomena. This paper deals with a mathematical model describing the SAR viewing geometry as a function of the off-nadir viewing angle. Quantitative results are obtained by simulating a spaceborne Tethered SAR Interferometer, which has been proposed for global topographic mapping. This system is based on two antennae, separated by a long flexible tether, with one transmitting and both receiving the return signal. A statistical approach is used to select the orbit which best fits the mission requirements and allows frequent observations. In particular, it is possible to access 95 percent of the Earth surface in less than 5 days.

Introduction

Currently, topographic mapping is particularly poor in several areas of the world and the existing cartography needs to be regularly updated. Furthermore, an accurate description of the surface elevation is of great importance to many branches of Earth sciences (Topographic Science Working Group, 1988). Among these, it is interesting to underline the need for high resolution digital elevation models (DEM) for natural disasters preparedness, prevention, and relief (Walter, 1989). In fact, Earth surface volumetric changes and small crustal motion are premonitory events of natural disasters such as floods, landslides, avalanches, volcanic eruptions, and earthquakes. On the other hand, mapping elevation changes caused by natural disasters allows for a more effective intervention (evacuation routes, sites for temporary dwellings, sources of water). As an example, many floods and alpine landslides follow from rapid snow melting, the study of which requires seasonal snow cover mapping at regional (100-m horizontal and 1 to 10-m vertical resolutions) and local (10-m horizontal and 0.1 to 1-m vertical resolutions) scales (Topographic Science Working Group, 1988). In addition, while topographic mapping requires global coverage, height measurements satisfying map accuracy standards (Welch and Marko, 1981; Doyle, 1982), and updating every 5 to 10 years, civil protection applications need frequent observations (every few days) of selected areas in order to compute height differences of the order of 1 to 10 centimetres.

As shown by Walter (1989), in addition to the knowledge of the DEM of the area under control, a high resolution image is required (e.g., 10 to 30 m resolution) to identify and classify various features of interest during and after a natural disaster. Due to space dynamics and data rate, a tradeoff between spatial and temporal resolution exists, which consists in decreasing the geometric resolution to increase the observation repetitivity (e.g., meteorological satellites) unless the sensor can vary the pointing angle of the aperture.

On the basis of several studies and requests, different space missions have been proposed for high resolution topographic mapping. They rely on different techniques such as stereo electro-optical sensors (Welch and Marko, 1981; Colvocoresses, 1982; Konecny *et al.*, 1987; Theodossiou and Dowman, 1990; Light, 1990), laser altimetry (Bufton, 1989; Gardner, 1992; Harding *et al.*, 1993), radargrammetry (Leberl, 1990), and Synthetic Aperture Radar (SAR) interferometry (Zebker and Goldstein, 1986; Gabriel and Goldstein, 1988; Prati *et al.*, 1990; Li and Goldstein, 1990).

SAR interferometry offers several advantages with respect to the other techniques such as night and day all-weather observation and output consisting of a DEM superimposed on a high resolution SAR image. Either a single antenna observing the same area from two orbits (separated in the cross-track direction) or two antennae operating simultaneously (single satellite or two satellites flying along parallel orbits) can be used for SAR interferometry. In the latter case, it is possible to overcome decorrelation problems which can significantly affect the DEM height accuracy (Zebker and Villasenor, 1992; Rodriguez and Martin, 1992). Moreover, using the Global Positioning System (Bertiger *et al.*, 1989) and/or on-board laser ranging sensors (Nerheim, 1990) for accurate estimation of the baseline, e.g., the distance between the two antennae foci (Li and Goldstein, 1990), mobile stations for rapid intervention can be envisaged, able to receive the data and generate real-time DEMs. Finally, differential interferometry allows one to map elevation changes at centimetric level by means of three SAR images of the same area separated in time and obtained with adequate baselines (Gabriel *et al.*, 1989; Monti Guarnieri *et al.*, 1992).

Various frequencies, from Ka to L-band, have been proposed for SAR interferometry. High repetitivity of the observation of selected areas requires electronic beem steering of the two SAR antennae, and this is more easily achieved at longer wavelenghts which, in addition, offer proven history of use both in space and in the ground segment.

This paper describes the mathematical model developed to evaluate the observation frequency of a spaceborne SAR Interferometer with off-nadir pointing capability (Figure 1).

Facoltà di Ingegneria, Università degli Studi di Napoli "Federico II," Piazzale Tecchio 80, 80125 Napoli, Italy.

Photogrammetric Engineering & Remote Sensing,
Vol. 61, No. 7, July 1995, pp. 891–898.

0099-1112/95/6107–891$3.00/0

Mathematical Model

Determination of Ascending and Descending Nodes

The satellite motion is described considering the secular perturbations of a Keplerian circular orbit, according to the first-order theory of Kozai (1959). These perturbations cause the perigee ($\dot{\omega}$) and the ascending node ($\dot{\Omega}$) precession, computed using the perturbed mean motion ($\dot{M}$).

The repetition factor (Q), defined for a repetitive orbit as the integer number of satellite revolutions (R) divided by the integer number of Earth rotations (N) with respect to the ascending node, is given by (Brooks, 1977)

$$Q=\frac{R}{N}=\frac{\dot{M}+\dot{\omega}}{\dot{\Lambda}-\dot{\Omega}} \tag{1}$$

where $\dot{\Lambda}$ is the Earth rotation rate.

In orbital mechanics, the ascending and descending nodes are defined with respect to the equatorial plane. In the following, we shall extend this wording to each parallel.

For each latitude, the repeating-trace pattern is computed considering the angle s between two adjacent ascending nodes (Duck and King, 1983): i.e.,

$$s=\frac{2\pi}{R} \tag{2}$$

and the angle s' between two successive ascending nodes:

$$s'=\frac{2\pi}{Q} \tag{3}$$

In each parallel plane, a polar reference frame is considered with origin in the parallel center (O) and with the x-axis directed towards the first ascending node (A_1). The angle of the nth ascending node (A_n) and the time elapsed ($\Delta t_{A_1 A_n}$) are given by

$$A_1\hat{O}A_n=(n-1)\frac{2\pi}{Q} \tag{4}$$

$$\Delta t_{A_1 A_n}=(n-1);\tau \tag{5}$$

where time is computed as a function of the nodal period (τ), which accounts for orbital perturbations.

The angle between the nth ascending and descending (D_n) nodes, as a function of the geocentric latitude (ϕ), depends on the satellite (subscript S) motion and the Earth (subscript $\leftrightharpoons$) rotation with respect to the nodal line

$$A_n\hat{O}D_n=A_n\hat{O}D_n|_S+A_n\hat{O}D_n|_{\leftrightharpoons} \tag{6}$$

where, with reference to Figure 2, i is the orbit plane inclination, the nodal line is defined as the intersection between the orbital plane and the equatorial plane, and

$$A_n\hat{O}D_n|_S=2\xi \tag{7}$$

$$A_n\hat{O}D_n|_{\leftrightharpoons}=\begin{cases} f\dfrac{2\pi}{Q} & \phi\geq 0 \\ (1-f)\dfrac{2\pi}{Q} & \phi<0 \end{cases} \tag{8}$$

$$f=\frac{\sin^{-1}(\cos\phi\sin\xi)}{\pi} \tag{9}$$

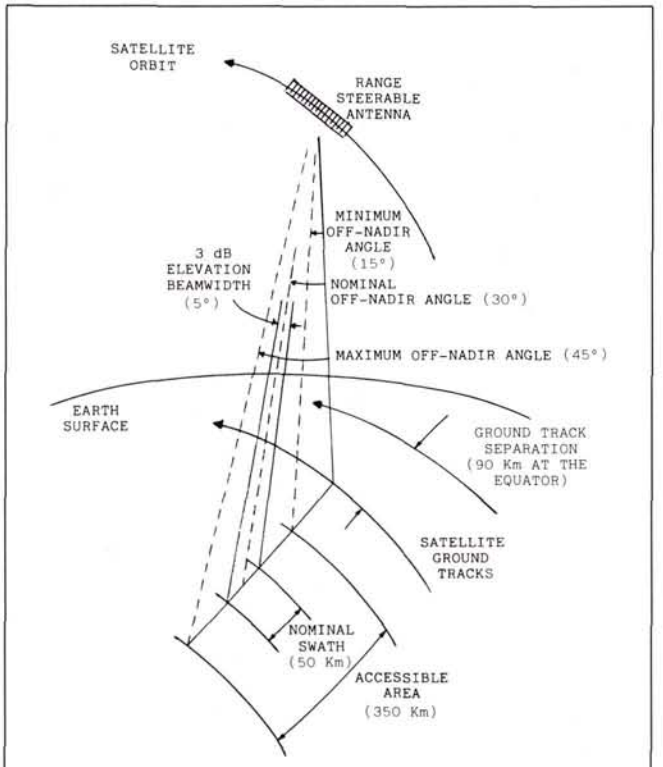

Figure 1. Swath width of a range steerable antenna.

$$\xi=\cos^{-1}\left(-\frac{\tan\phi}{\tan i}\right) \tag{10}$$

The corresponding time interval is computed as follows:

$$\Delta t_{A_nD_n}=\begin{cases} f\tau & \phi\geq 0 \\ (1-f)\tau & \phi<0 \end{cases} \tag{11}$$

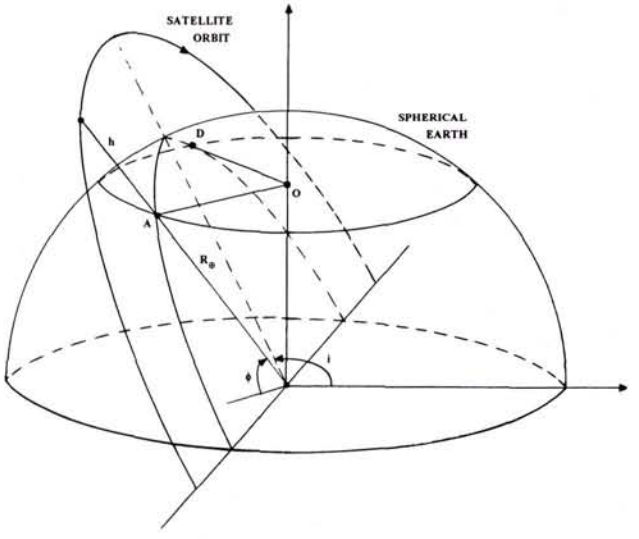

Figure 2. Orbital geometry.

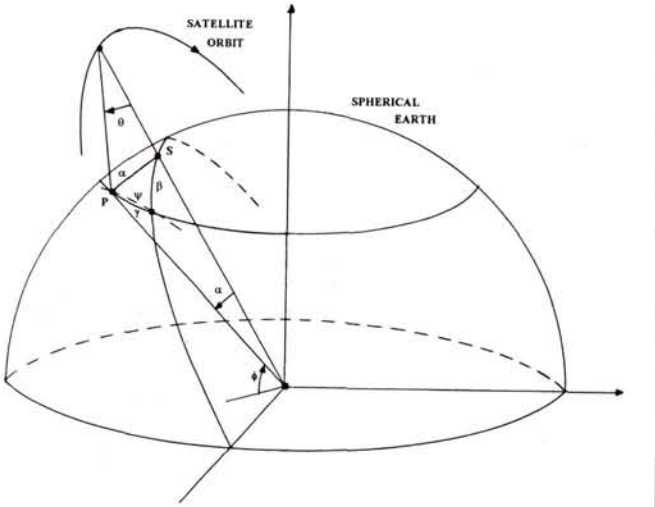

Figure 3. Satellite viewing geometry.

The results presented in King (1976), which mainly address the problem connected to the equatorial coverage, can be obtained by introducing $\phi=0$ in Equations 6 to 10.

Observation Geometry

The observation geometry of the satellite is analyzed to compute the angle subtended by the arc between the two points on the parallel corresponding to the minimum and maximun off-nadir viewing angles.

With reference to Figure 3, the off-nadir viewing angle (ϑ), at which a point P on the Earth at latitude ϕ is observed, corresponds to the geocentric angle (α) between the subsatellite point (S) and the observed point (P) as follows:

$$\alpha=\sin^{-1}\left\{\frac{\sin\vartheta}{R^{\oplus}}\left[(R^{\oplus}+h)\cos\vartheta-\sqrt{(R^{\oplus}+h)^2\cos^2\vartheta-h^2-2R^{\oplus}h}\right]\right\} \quad (12)$$

where $R^{\oplus}$ is the spherical Earth radius and h is the satellite altitude.

Neglecting Earth rotation, an assumption which later will be removed, the angle (γ) lying in the parallel plane between the satellite crossing point at the same latitude of P and P itself is given by

$$\gamma=\cos^{-1}\left(1-\frac{1-\cos\psi}{\cos^2\phi}\right) \quad (13)$$

where ψ is the great circle arc

$$\psi=\cos^{-1}\left(\frac{-\sin\alpha\,\sin\phi\,\cos i+\sin^2\phi+\sqrt{\Delta^*}}{\sin^2 i}\right) \quad (14)$$

and

$$\Delta^*=(\sin^2 i-\sin^2\phi)(-\sin^2\alpha+2\sin\alpha\,\sin\phi\,\cos i+\sin^2 i-\sin^2\phi) \quad (15)$$

The geocentric angle (β) between the sub-satellite point (S) and the crossing point at the same latitude of the observed point P is

$$\beta=\cos^{-1}\left(\frac{\cos\psi}{\cos\alpha}\right) \quad (16)$$

The angular position of point P with respect to the ascending/descending nodes is then obtained considering the contribution due to γ and the additional term due to the Earth rotation as a function of the angle β: i.e.,

$$A_n\hat{O}P=\gamma(\vartheta)+\beta(\vartheta)\frac{g}{Q} \quad (17)$$

where

$$g=\begin{cases}+1 & i\geq 90 \text{ deg}\\ -1 & i<90 \text{ deg}\end{cases} \quad (18)$$

The same analysis can be performed to derive the angular position of a point observed during the descending phase of the orbit. In this case, the angle ($P\hat{O}D_n$) is obtained by Equation 17 changing the sign of the second member.

The difference between Equation 17 computed for the maximum and minimum off-nadir viewing angles gives the intersection of the potential swath width with the parallel at latitude ϕ. In addition, by adding Equations 4 and 17, it is possible to determine the swath intersection with respect to the first ascending node.

The derived equations can be applied when the sub-satellite geocentric latitude (referred to as ϕ_s) is

$$|\phi_s|\leq\begin{cases}i & i\leq 90 \text{ deg}\\ 180-i & i>90 \text{ deg}\end{cases} \quad (19)$$

and, consequently, the limitations on the observed parallel latitude can be calculated by the following equation:

$$\phi_s=\sin^{-1}(\cos\beta\sin\phi+g\sin\beta\sqrt{\sin^2 i-\sin^2\phi}) \quad (20)$$

The above model has been derived considering a positive off-nadir viewing angle with respect to a satellite-fixed right-handed reference frame. In the case of a negative angle, the equations are quite similar, so their derivation will be omitted for the sake of brevity.

TABLE 1. ORBIT MAIN PARAMETERS

repetition factor Q	orbit altitude h (km)	orbit inclination i (deg)	nodal period τ (s)	equatorial adjacent track distance (Km)
412/27	482.00	97.339	5662.1	97.270
413/27	470.90	97.298	5648.4	97.034
415/27	448.82	97.215	5621.2	96.566
416/27	437.86	97.175	5607.7	96.334
418/27	416.05	97.094	5580.9	95.873
429/28	463.39	97.270	5639.2	93.415
431/28	442.16	97.190	5613.0	92.952
433/28	421.10	97.113	5587.1	92.552
440/29	508.21	97.438	5694.6	91.080
441/29	497.77	97.399	5681.6	90.873
442/29	487.37	97.360	5668.8	90.668
443/29	477.02	97.321	5656.0	90.463
444/29	466.70	97.282	5643.2	90.259
445/29	456.42	97.243	5630.6	90.056
446/29	446.17	97.205	5617.9	89.854
447/29	435.97	97.168	5605.4	89.653
448/29	425.80	97.130	5592.9	89.453
449/29	415.67	97.093	5580.4	89.254
457/30	489.80	97.369	5671.8	87.692
461/30	449.92	97.219	5622.6	86.931
463/30	430.20	97.146	5598.3	86.555

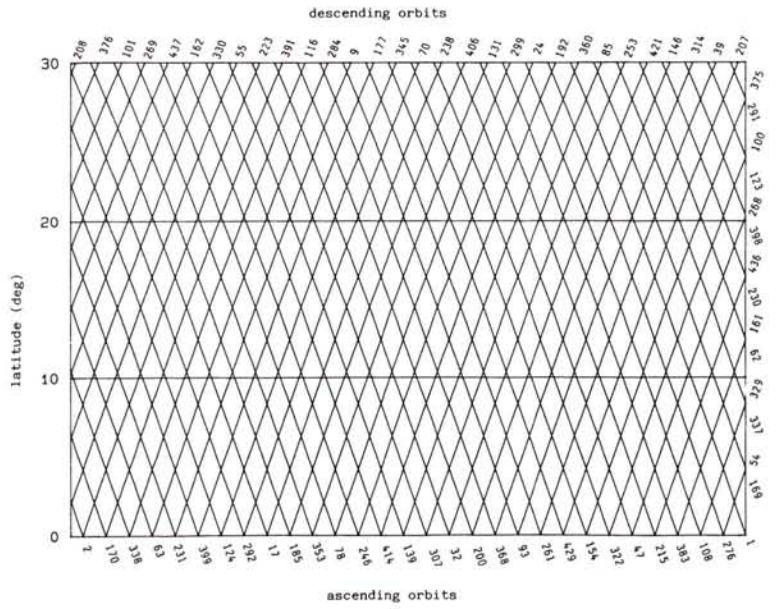

Figure 4. Orbit 443/29 ascending and descending ground tracks.

Application of the Model

Orbit and Off-Nadir Angles Selection

This model has been applied to study a preliminary configuration of a Tethered SAR Interferometer in sun-synchronous orbit at an altitude of about 450 km (Moccia and Vetrella, 1992). This system is based on two antennae, separated by a long flexible tether, with one transmitting and both receiving the return signal. In order to reduce tether longitudinal oscillations due to thermal effects and to simplify the solar panel orientation, the ascending node is at 6 PM local time. A nominal 50-km cross-track swath width is achieved by means of an L-band antenna elevation beamwidth of 5.3 degrees and a positive side-looking angle of 25 degrees, which has been chosen to increase the SAR coverage of Antarctica.

As a consequence of the selected swath width and altitude, global coverage cannot be achieved in less than 27 days. A longer period allows a reduction of the swath width and data rate, but it is less effective with regard to repetitivity. Consequently, only orbits with repetition period between 27 and 30 days have been considered.

For a given Q and assuming in Equation 1 the satellite ascending node precession equal to the sun precession (0.9856 deg/day), an iterative procedure allows one to derive the sun-synchronous altitude and inclination of the 21 orbits which will be considered in the following (Table 1).

Range beam electronic steering is used to vary the off-nadir viewing angle between 15 and 45 degrees, increasing the real 50-km swath to a potential swath of about 350 km (Figure 1). Observation frequency could be increased by selecting a larger interval, but we chose this value considering the off-nadir angles proposed for various spaceborne SARs (Way and Smith, 1991).

Of course, the look angle variation causes differences in resolution and accuracy of the interferometric SAR. However, possible drawbacks can be overcome. For instance, by means of a digital chirp generator, it is possible to change the range chirp bandwidth in order to keep planimetric resolution constant along the potential swath.

Off-nadir angle variation involves differences in the unavoidable geometric distortion of SAR images such as foreshortening, layover, and shadow (Curlander and McDonough,

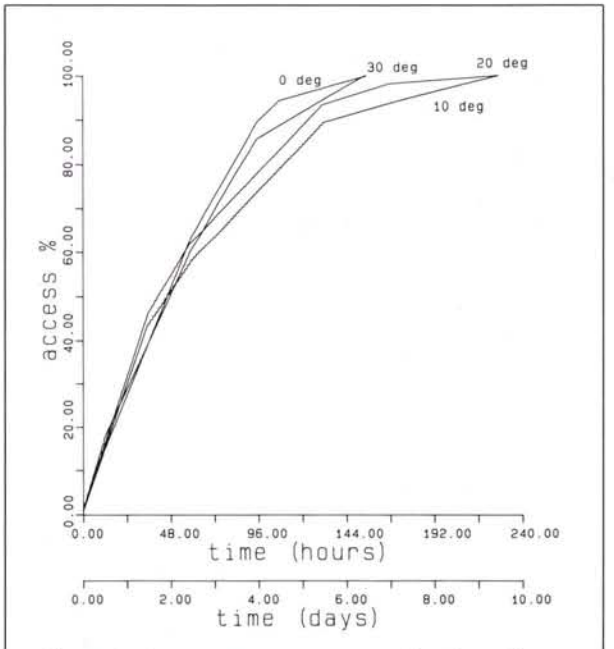

Figure 5. Access percentage as a function of time (orbit 443/29).

TABLE 2a. MAXIMUM ACCESS ACQUISITION TIME AS A FUNCTION OF LATITUDE

latitude ϕ (deg)	100% access acquisition time (hours)										
	Q=412/27	Q=413/27	Q=415/27	Q=416/27	Q=418/27	Q=429/29	Q=431/28	Q=433/28	Q=440/29	Q=441/29	Q=442/29
70	63.1	62.9	54.7	54.5	102.3	54.8	54.6	54.3	87.2	71.2	71.0
60	80.2	80.0	104.6	104.4	248.0	70.7	104.5	152.1	109.4	95.0	85.3
50	94.7	132.1	81.2	118.7	320.9	131.9	81.1	176.9	84.2	84.0	94.8
40	177.7	155.8	129.6	118.8	203.5	155.5	129.4	155.6	131.7	107.8	203.6
30	154.1	166.8	178.0	274.2	489.9	395.3	297.8	298.0	129.7	118.9	227.3
20	322.4	130.2	155.2	322.4	323.1	274.1	275.0	179.1	143.0	119.0	347.0
10	323.1	203.1	154.6	370.7	370.5	274.8	311.0	226.6	203.2	119.1	346.4
0	107.0	178.9	178.8	274.9	490.7	394.7	322.7	298.8	227.0	131.0	130.7
−10	275.2	154.6	203.0	226.7	298.5	298.5	131.0	202.6	250.8	322.8	298.5
−20	274.6	155.3	191.5	119.3	347.3	299.2	119.5	203.3	131.3	226.7	299.2
−30	95.4	178.3	179.6	155.8	514.2	250.1	119.5	274.2	107.6	130.5	95.5
−40	132.1	131.8	154.2	119.5	225.9	275.7	153.9	178.0	83.8	119.5	153.9
−50	108.5	71.8	105.8	119.6	372.1	71.7	105.7	228.1	81.9	81.7	177.6
−60	81.5	81.3	60.9	60.8	105.2	71.8	60.8	105.3	120.0	105.5	85.0
−70	61.3	61.2	37.5	48.2	47.9	37.6	37.4	47.9	61.7	61.6	61.4
maximum time	323.1	203.1	203.0	370.7	490.7	395.2	322.7	298.8	250.8	322.8	347.0

TABLE 2b. MAXIMUM ACCESS ACQUISITION TIME AS A FUNCTION OF LATITUDE

Latitude ϕ (deg)	100% access acquisition time (hours)									
	Q=443/29	Q=444/29	Q=445/29	Q=446/29	Q=447/29	Q=448/29	Q=449/29	Q=457/30	Q=461/30	Q=463/30
70	63.0	54.9	54.7	54.6	54.5	54.4	102.3	71.1	54.7	54.4
60	80.1	79.9	70.6	104.6	104.3	104.1	248.0	85.3	61.1	104.2
50	132.3	132.0	153.3	81.1	129.2	177.1	355.0	60.2	81.2	129.1
40	156.0	155.6	201.8	129.5	107.9	107.6	203.5	203.7	129.6	107.7
30	154.0	238.8	394.1	177.9	274.0	202.0	537.9	131.3	178.0	202.2
20	226.2	202.2	299.3	155.1	202.4	179.3	323.0	214.9	155.2	131.2
10	226.9	202.9	298.7	191.1	250.7	178.7	418.5	250.5	154.6	167.1
0	154.8	250.8	394.9	191.2	274.8	250.9	538.7	130.8	178.8	370.9
−10	167.4	226.6	347.2	131.1	226.6	154.7	298.5	202.5	203.0	215.5
−20	167.5	227.3	346.6	179.5	119.3	155.4	395.3	203.2	202.4	155.5
−30	106.3	178.2	251.8	179.5	155.7	203.5	514.1	130.2	179.6	167.4
−40	132.0	203.8	298.3	154.1	119.5	130.1	225.9	154.0	154.2	130.2
−50	108.4	71.8	71.6	105.8	119.6	180.2	420.1	119.4	105.9	132.2
−60	81.4	71.9	71.7	60.9	60.7	60.6	105.2	95.9	60.9	60.6
−70	61.3	61.1	37.5	37.5	48.1	48.0	47.9	61.4	37.5	48.0
maximum time	226.9	250.8	394.9	191.2	274.8	250.9	538.7	250.5	203.0	370.9

TABLE 3. TIME INTERVALS REQUIRED TO OBSERVE 80, 95, AND 100 PERCENT OF THE RANDOMLY DISTRIBUTED POINTS

observed points	orbit (Q)	time interval (hours)				
		observation 1	observation 2	observation 3	observation 4	observation 5
80%	413/27	72.2	144.4	221.4	304.6	376.8
	415/27	76.4	151.3	235.6	319.8	397.8
	443/29	70.7	138.2	218.2	292.0	370.5
	446/29	76.4	145.1	240.2	308.9	405.6
	461/30	76.4	154.4	229.3	316.7	394.7
95%	413/27	127.2	193.1	303.0	376.8	445.9
	415/27	131.0	184.1	304.2	374.4	457.1
	443/29	117.8	180.6	271.6	372.1	434.9
	446/29	120.1	181.0	293.3	365.0	464.9
	461/30	138.8	191.9	308.9	400.9	460.2
100%	413/27	229.2	266.9	464.7	480.4	635.9
	415/27	251.2	263.6	443.0	516.4	636.5
	443/29	252.8	263.8	423.9	444.3	588.8
	446/29	290.2	312.0	491.4	503.9	683.3
	461/30	252.7	263.6	444.6	517.9	636.5

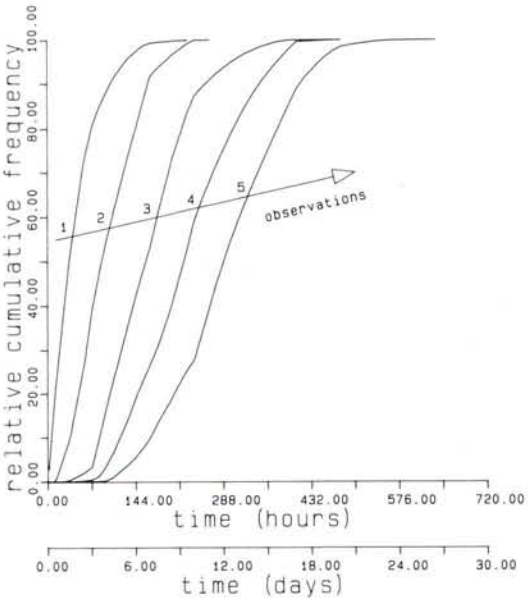

Figure 6. Relative cumulative frequency as a function of time (orbit 413/27).

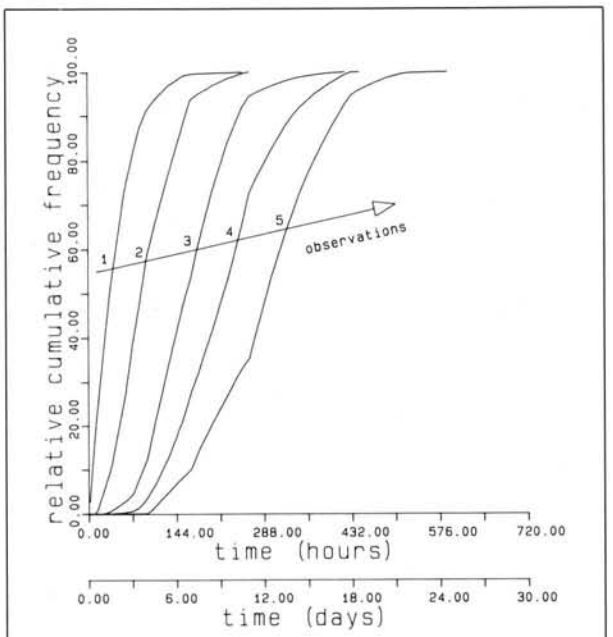

Figure 7. Relative cumulative frequency as a function of time (orbit 443/29).

1991). On the other hand, various algorithms which account for these aspects have been proposed (Goldstein *et al.*, 1988; Prati *et al.*, 1990; Lin *et al.*, 1992).

With reference to the DEM height accuracy, the dependence on the off-nadir angle is of minor importance with respect to other factors, such as baseline indetermination and inaccuracy, signal-to-noise ratio, and chirp sampling frequency (Li and Goldstein, 1990; Moccia and Vetrella, 1992). Consequently, adequate system design and data processing allow one to achieve a satisfactory height error budget (Rodriguez and Martin, 1992).

Numerical Results

Taking into account the computing time to simulate global access, a preliminary parametric study has been conducted to determine the time intervals required to obtain the complete access of the parallels, using the 30-degree potential antenna beamwidth, at latitudes ranging from −70 to +70 degrees with a 10-degree step. Because in proximity of the Earth poles the satellite ground tracks are closer and repetitivity increases significantly, we restricted our analysis to this more populated range of latitudes.

The access is computed by adding the swath width intersection (Equations 4, 6, and 17) relative to each ascending and descending node. The time intervals are shown in Tables 2a and 2b, where the maximum values for each selected orbit are also listed. These "worst case" values are related to the first observation of a random point at the selected latitudes after the occurrence of a natural disaster.

Referring to Tables 2a and 2b, it is worth noting that in several cases 100 percent access acquisition time does not decrease with the absolute magnitude of latitude. This is due to the variation with latitude of the descending node grid with respect to the ascending one, as it results from Equations 6 to 10. Because of access dependence on ascending and descending grid relative position (Equations 17, 4, and 6), a small variation of latitude may cause significant access variation.

This effect has been put in evidence in Figure 4, which shows the ground tracks of ascending and descending orbits in the latitude interval 0 to 30 degrees and in the longitude interval between the first and the second ascending tracks. In Figure 5, the percentage of accessed areas at latitudes 0, 10, 20, and 30 degrees are plotted. Whereas in Figure 4 the track interceptions at the different latitudes are nearly similar from a geometrical point of view, they differentiate in orbit numbers. Because time is proportional to orbit numbers, the swath widths will intercept each other in a sequence strongly dependent on the nodes sequence. Consequently, the advantage connected to increasing latitude (reduced length of the parallel) can be partially or totally removed (Figure 5). Of course, during the first hours, when no interception occurs, this effect is not yet present.

The above considerations imply that the proposed parametric analysis might be misleading if used without any further investigation. On the other hand, it has the advantage of an extremely reduced computing time and it can be used to neglect those orbits which certainly do not offer an adequate observation frequency. Consequently, only five orbits, characterized by a maximum time interval of the order of 200 hours (Tables 2a and 2b), have been analyzed more thoroughly. One hundred thousand points on the Earth's surface have been extracted randomly from a uniform distribution, within longitude and latitude ranging from −180 to +180 degrees and from −70 and +70 degrees, respectively. The antenna steering allows observation of a point only if it is within the intersection of the potential swath width and the parallel where the point is located. By means of an iterative procedure based on the mathematical model, the off-nadir viewing angles, at which each point is observed, are com-

puted. Of course, the highest probability of observation occurs at large off-nadir angles, because the swath width is wider.

The time intervals necessary to obtain the consecutive observations are computed by using Equations 5 and 11. Table 3 shows the time intervals required to observe 80, 95, and 100 percent of the randomly distributed points for the first five times. These values have been chosen because they give an effective estimate of the orbit performance. It is interesting to note that the slope of the relative cumulative frequency curves decreases significantly in proximity of 100 percent observed points. Finally, Figures 6 and 7 show the cumulative frequencies for the orbits 413/27 and 443/29. They have comparable values of altitude and inclination and offer 36.5 percent (5.0 percent) of probability to observe once (twice) a natural disaster within the first 24 hours, and 62.6 percent (18.6 percent) within the first 48 hours. The first orbit allows observation of 100 percent of the points in the shortest time (Table 3), while the second offers a better observation frequency which is particularly useful for natural disaster management. Finally, it is worth noting that the more comprehensive analysis of the two orbits does not significantly modify the preliminary results of Tables 2a and 2b.

Conclusions

This paper has shown that a spaceborne SAR interferometer, with two antennae operating simultaneously and the additional capability of range beam electronic steering, offers an observation frequency of selected areas which represents a significant improvement with respect to existing and proposed spaceborne systems and, consequently, can be of great interest for natural disaster prevention, preparedness, and relief. In addition to conventional high resolution SAR images, the interferometric technique provides the capability for measuring the height of the ground and monitoring time-varying phenomena when volume change detection is required.

To analyze the potential observation frequency of such a system, a model of general validity has been developed, which can be used to study other space remote sensing missions. This model accounts for first-order orbital perturbations, satellite-Earth relative motion, observed area latitude, and off-nadir viewing angle.

On the basis of mission requirements which were identified during the feasibility study of a spaceborne Tethered Interferometric SAR, a numerical simulation was carried out to select the orbit with a repetitivity factor adequate for global topographic mapping which optimizes the time interval between successive observation of a selected area.

Future research activities will focus on the analysis of new space configurations, such as SAR interferometry by two free- flying satellites in parallel orbits, and on the observation frequency obtainable on a limited number of test-sites where high probability of natural disaster occurence exists.

Acknowledgments

This paper has been supported by the financial contribution of the Italian Space Agency (ASI) and of the Italian Ministry for University and Research.

References

Bertiger, W.I., S.M. Lichten, and E.C. Katsigris, 1989. A demonstration of sub-meter GPS orbit determination and high presition user positioning, *IEEE Transactions on Aerospace and Electronic Systems*, 4(2):16–25.

Brooks, D.R., 1977. *An Introduction to Orbit Dynamics and Its Application to Satellite-Based Earth Monitoring Mission*, NASA RP-1009, Washington, D.C.

Bufton, J.L., 1989. Laser altimetry measurements from aircraft and spacecraft, *Proceedings of the IEEE*, 77(3):463– 477.

Colvocoresses, A.P., 1982. An Automated Mapping Satellite System (Mapsat), *Photogrammetric Engineering & Remote Sensing*, 48(10):1585–1591.

Curlander, J.C., and R.N. McDonough, 1991. *Synthetic Aperture Radar*, John Wiley & Sons, New York, N.Y., 647 p.

Doyle, F.J., 1982. Mapping control for remotely sensed data, *Proceedings of the XVIth International Symposium on Remote Sensing of the Environment*, Cairo, Egypt, pp. 111–120.

Duck, K.I., and J.C. King, 1983. Orbital Mechanics for Remote Sensing, *Manual of Remote Sensing, Second Edition* (R.N. Colwell, editor), American Society of Photogrammetry, Falls Church, Virginia, Vol. 1, pp. 704.

Gabriel, A.K., and R.M. Goldstein, 1988. Crossed orbit interferometry: theory and experimental results form SIR-B, *International Journal of Remote Sensing*, 9(8):857–872.

Gabriel, A.K., R.M. Goldstein, and H.A. Zebker, 1989. Mapping small elevation changes over large areas: differential radar interferometry, *Journal of Geophysical Research*, 94(B7):9183–9191.

Gardner, C.S., 1992. Ranging Performance of Satellite Laser Altimeters, *IEEE Transaction on Geoscience and Remote Sensing*, 30(5):1061–1072.

Goldstein, R.M., H.A. Zebker, and C. Werner, 1988. Satellite radar interferometry: two dimensional phase unwrapping, *Radioscience*, 23(4):713–720.

Harding, D.J., J.L. Bufton, and J.J. Frawley, 1993. Satellite Laser Altimetry of Terrestrial Topography: Vertical Accuracy as a Function of Surface Slope, Roughness, and Cloud Cover, Submitted to *IEEE Transaction on Geoscience and Remote Sensing*.

King, J.C., 1976. Quantization and Symmetry in Periodic Coverage Patterns with Applications to Earth Observation, *The Journal of Astronautical Sciences*, 24(4):347–63.

Konecny, G., P. Lhoman, H. Engel, and E. Kruck, 1987. Evaluation of SPOT Imagery on Analytical Photogrammetric Instruments, *Photogrammetric Engineering & Remote Sensing*, 53(9):1223–1230.

Kozai, Y., 1959. The Motion of a Close Earth Satellite, *The Astronomical Journal*, 64(1274):367–377.

Leberl, W.F., 1990. *Radargrammetric Image Processing*, Artech House, Norwood, Massachusetts, pp. 595.

Li, K., and R.M. Goldstein, 1990. Studies of Multibaseline Spaceborne Interferometric Synthetic Aperture Radar, *IEEE Transaction on Geoscience and Remote Sensing*, 28(1):88–97.

Light, D.L., 1990. Characteristics of Remote Sensors for Mapping and Earth Science Applications, *Photogrammetric Engineering & Remote Sensing*, 56(12):1613–1623.

Lin, Q., J.F. Vesecky, and H.A. Zebker, 1992. New Approaches in Interferometric SAR Data Processing, *IEEE Transactions on Geoscience and Remote Sensing*, 30(3):560–567.

Monti Guarnieri, A., F. Parizzi, P. Pasquali, C. Prati, and F. Rocca, 1992. Developments in ERS-1 SAR Interferometry, *Proceedings of 1st Workshop ESA ESRIN*, Frascati, Italy, pp. 13.

Moccia, A., and S. Vetrella, 1992. A Tethered Interferometric Synthetic Aperture Radar (SAR) for a Topographic Mission, *IEEE Transaction on Geoscience and Remote Sensing*, 30(1):103–109.

Moccia, A., S. Vetrella, and M. Grassi, 1992. Attitude Dynamics and Control of a Vertical Interferometric Radar Tethered Altimeter, *AIAA Journal of Guidance, Control, and Dynamics*, 16(2):264–269.

Nerheim, N., 1990. *Conceptual Design of an Antenna Position Sensor for the GLAM-VISTA (Global Topography Mission-Vertical*

Interferometric SAR Tethered Altimeter) Mission, Jet Propulsion Laboratory, Interoffice Memo 343-90-283, 9 p.

Prati, C., F. Rocca, A. Monti Guarnieri, and E. Damonti, 1990. Seismic Migration for SAR Focusing: Interferometrical Applications, *IEEE Transactions on Geoscience and Remote Sensing*, 28(4): 627–639.

Rodriguez, E., and J.M. Martin, 1992. Theory and design of interferometric synthetic aperture radars, *IEEE Proceedings-F*, 139(2):147–159.

Theodossiou, E.I., and I.J. Dowman, 1990. Heighting Accuracy of SPOT, *Photogrammetric Engineering & Remote Sensing*, 56(12): 1643–1649.

Topographic Science Working Group, 1988. *Topographic Science Working Group Report to the Land Processing Branch, Earth Science and Application Division, NASA Headquarters*, Lunar and Planetary Institute, Houston, 64 p.

Way, J., and E. Atwood Smith, 1991. The Evolution of Synthetic Aperture Radar Systems and their Progression to the EOS SAR, *IEEE Transaction on Geoscience and Remote Sensing*, 29(6):962–985.

Welch, R., and, W. Marko, 1981. Cartographic Potential of a Spacecraft Line-Array Camera System: Stereosat, *Photogrammetric Engineering & Remote Sensing*, 47(8):1173–1185.

Walter, L.S., 1989. Application of Satellite Technology to Disaster Management. *Communication when it's Needed Most*, The Anneberg Washington Program in Communications Policy Studies of Northwestern University (David Webster, editor), pp. 74–93.

Zebker, H.A., and R.M. Goldstein, 1986. Topographic Mapping from Interferometric Synthetic Aperture Radar Observations, *Journal of Geophysical Research*, 91(B5):4993–4999.

Zebker, H.A., and J. Villasenor, 1992. Decorrelation in Interferometric Radar Echoes, *IEEE Transactions on Geoscience and Remote Sensing*, 30(5):950–959.

(Received 2 December 1992; revised and accepted 23 June 1993; revised 12 August 1993)

Marco D'Errico
Marco D'Errico received the doctoral degree in aeronautical engineering in 1992 from the University of Naples, Italy. He is currently a Ph.D. student in Aerospace Engineering at the University of Naples, developing his research activity within the Global Topography Mission project.

Antonio Moccia
Since 1990 Antonio Moccia has been professor of aerospace servosystems at the Faculty of Engineering in Naples, Italy. His research activities deal with aerospace high resolution remote sensing systems design and data processing, and tethered systems dynamics and control. He is member of the NASA/ASI Global Topography Mission Working Group, and since 1975 he has held several grants and research contracts from the National Research Council, the University of Naples, the Italian Space Agency, Alenia Spazio, and Telespazio.

Sergio Vetrella
Since 1972 Sergio Vetrella has been the principal investigator of several national and international programs of research in the field of aerospace remote sensing systems. Since 1977 he has been a professor of space systems engineering at the Faculty of Engineering in Naples, Italy. He has been a member of the Scientific Committee of the Italian Space Agency since 1989. He is also president of the Consortium CO.RI.S.T.A., a consortium for the research and development of advanced remote sensing systems.